Double-layer formation and propulsive assessment for a three-species plasma expanding in a magnetic nozzle

Eduardo Ahedo[a)]
ETS Ingenieros Aeronáuticos, Universidad Politécnica de Madrid, Madrid 28040, Spain

(Received 22 October 2010; accepted 23 February 2011; published online 29 March 2011)

The quasi one-dimensional expansion of a collisionless plasma with a hot-electron tail in a gentle convergent-divergent nozzle is studied. A parametric investigation of the plasma response is carried out in terms of the relative density and temperature of the hot-electron population. The formation of a steepened layer is shown to be due to the anomalous thermodynamic behavior of the plasma, which creates a local minimum of the Mach number. The change from a quasineutral to a non-neutral steepened layer occurs when this minimum goes below one and several sonic points appear. The non-neutral double layer does not introduce further changes in the plasma response. All gain in plasma momentum and thrust is related to the supersonic expansion in the divergent nozzle, with zero contribution of the double layer. A comparative analysis of thrust efficiency of plasmas with and without hot electrons does not find any gain in the presence of hot electrons; instead, a small penalty in the expansion efficiency seems to exist. The study is limited to Maxwellian electron populations and finite nozzles. © *2011 American Institute of Physics*.
[doi:10.1063/1.3567159]

I. INTRODUCTION

Space plasma thrusters based on helicon sources are a subject of current research.[1–4] In its simplest design, a helicon thruster consists of a discharge chamber and a magnetic nozzle. The chamber is a cylindrical helicon source where the plasma is produced and heated. Then, the magnetic nozzle transforms the plasma internal energy into a supersonic ion beam, with the aid of the ambipolar electric field.[5–7] The helicon thruster is an electrothermal thruster and no external cathode is needed to neutralize the ejected current-free plasma.

Charles and Boswell reported the formation of a current-free double layer (CFDL) near the interphase of a helicon source and a larger diffusion chamber[1] and related the presence of a supersonic ion beam to the jump in electric potential across the CFDL.[8] These experiments aroused a large expectation because it was suggested that 'the CFDL in an expanding plasma could be the basis of an enhanced type of space plasma thruster',[1] referred to later as the Helicon Double Layer Thruster (HDLT).[9]

A double layer (DL) consists of a positive and a negative Debye sheath, connecting two quasineutral regions of the plasma. Because of its thinness, the double layer is observed as a jump in the profiles of the electric potential and the plasma density; theoretical models invoke the zero Debye length limit and treat the DL as a discontinuity in the quasineutral plasma. The CFDL is a particular case of DL known from studies on the expansion of laser-produced plasma coronas[10–12] and material processing with electronegative plasmas.[13–16] In *all* these studies, the CFDL is formed within a plasma that contains two negative species *with disparate temperatures*, and for a limited range of the density ratio of these species. It makes basically no difference whether these species are either electrons and (cold) negative ions or cold and hot electrons. An excellent experiment on the formation and properties of a CFDL is due to Hairapetian and Stenzel,[17] who studied the expansion of a collisionless plasma with a controlled population of hot electrons, about 20 times hotter than the main electron population. They demonstrated (i) the direct relation between the presence of hot electrons and the formation of a steepened potential profile, and (ii) the scaling of the supersonic ion beam energy with the hot-electron temperature.

In addition to the Charles–Boswell experiment, the presence of a CFDL has been claimed in other helicon sources.[18–20] Also, a hot-electron tail has been reported in several helicon-based plasmas.[19,21–24] However, important issues related to both the CFDL properties and its relevance as a propulsion mechanism remain unanswered. First, the CFDL does not form in all helicon source experiments and the same seems to be true with respect to the hot-electron tail. Thus, the operational conditions that assure the presence of the hot-electron tail and the CFDL and the connection between these two phenomena must be clarified.

Second, it is uncertain whether the Charles–Boswell DL is identical to the Hairapetian–Stenzel one. In the last case, all the plasma is produced upstream and then expanded into vacuum (which is also the desirable scenario for a space plasma thruster). In the Charles–Boswell experiment, there is a significant plasma production downstream the DL, which leads to an extra population there of trapped low-energy ions and additional cold electrons that are likely to have some effect on the DL formation.

Third, the CFDL is a weak type of double layer, in the sense that the degree of non-neutrality (measured as the ratio of the electric charge density to the dominant plasma density) is small (~0.4% in the Hairapetian–Stenzel experi-

[a)]Electronic mail: eduardo.ahedo@upm.es.

ment). This makes the DL extend tens or hundreds of Debye lengths. As a consequence, in real experiments where the Debye length is finite, the distinction between a non-neutral layer and a mere quasineutral steepened layer (QSL) is unclear.

Fourth, a supersonic ion beam does not prove the presence of a CFDL, since a quasineutral plasma also becomes supersonic when expanding along a convergent-divergent magnetic nozzle, as Andersen *et al.* demonstrated experimentally.[6] Furthermore, a double layer is known to conserve the plasma momentum[25–27] so no thrust enhancement is expected from it.[28] This raises the question of whether a CFDL has any propulsive role or, more generally stated, whether the presence of a hot-electron tail yields any propulsive gain to the plasma thruster.

In a recent letter,[29] Ahedo and Martínez-Sánchez analyzed the formation of a CFDL in a collisionless fully-ionized plasma with a hot-electron tail (which we call a *three-species* plasma) flowing in a convergent-divergent nozzle. The DL was shown to be a limit case of a QSL. The DL characteristics were different depending on whether it formed at the nozzle divergent side, convergent side, or throat. The connection of each type with previous CFDL studies on other applications was established. The CFDL formed in the divergent nozzle agrees well with the Hairapetian–Stenzel DL and is the most interesting case for plasma thrusters.

This paper extends the study initiated in that letter with several goals. The first one is to interpret the formation of a QSL and a CFDL in terms of the peculiar thermodynamics of a three-species plasma, and to show that the CFDL forms when the quasineutral solution presents several sonic points, and only one can be crossed regularly. This result contrasts sharply with recent studies by Fruchtman[28] and Chen.[30] Fruchtman claims that a CFDL is formed in a *simple* (i.e., two-species) plasma when there are abrupt changes of the nozzle shape or localized ionization. Chen claims that 'the "double layers" of Charles *et al.* are actually single layers and are predictable from classical sheath theory'.

The second goal of our study is to discuss (within a unique model) the respective roles of the DL and the magnetic nozzle on enhancing the momentum flux of a three-species plasma. The plasma downstream velocity and momentum flux measure, respectively, the specific impulse and thrust of the propulsive device ejecting the plasma. The third goal is to discuss whether the presence of a DL or, more generally, a hot-electron tail brings any propulsive gain over a simple plasma.

The paper layout is as follows. Section II presents the one-dimensional (1D) model of Ref. 29 and discusses the anomalous thermodynamics of the fluid representing the three-species plasma. Section III discusses the different regimes, with and without DL, in terms of plasma properties. Section IV analyzes, first, the spatial variation of the ion and electron momenta in DL and nozzle, and second, discusses the thrust efficiency of three-species and simple plasmas for similar thruster operation conditions. Conclusions are in Sec. V. An Appendix, based on Ref. 29, explains how the DL solutions are obtained.

II. MODEL FORMULATION

As in Ref. 29, we consider a collisionless, fully-ionized, three-species plasma, constituted of singly-charged ions (i) and cold (c) and hot (h) electron populations satisfying the Boltzmann relation. This plasma is accelerated through a convergent-divergent magnetic nozzle, whose cross-section area, $A(z)$, varies gently. Furthermore, we expect dA/dz to increase in the divergent side of a magnetic nozzle, which assures supersonicity.

An asymptotic two-scale analysis is carried out, based on the length hierarchy

$$\lambda_D \ll \ell_e \ll L \ll \lambda_{col},$$

with $L \sim dz/d\ln A$ the nozzle divergence length, ℓ_e the electron gyroradius, and λ_{col} the shortest mean-free path of possible collisional processes.

This simplified and partial model of the plasma discharge is thought suitable enough for providing a correct response to the goals enumerated above. A full and consistent model of the plasma thruster discharge should include: (1) the plasma ionization and heating processes, taking place at the upstream region of the nozzle, (2) a better kinetic model for electrons, (3) the two-dimensional aspects of the plasma expansion, and (4) the nozzle/plasma detachment, at the downstream end of the nozzle. The upstream plasma region for the case of a helicon thruster was treated by Fruchtman *et al.*[31] and Ahedo.[32] The loss of the Maxwellian character of collisionless electrons due to the combination of electrostatic barriers and inverse magnetic mirror effects has been treated, for a simple plasma, by Arefiev and Breizman, who also suggested the electron adiabatic cooling caused by the expansion of the plasma plume boundary.[33] A two-dimensional (2D) model of the supersonic expansion of a collisionless plasma in a divergent magnetic nozzle was developed by Ahedo and Merino.[7] An important result, which supports the present study, is that a quasi-1D model, although ignoring radial gradients and electric currents, approximates well the radially-averaged behavior of the 2D response of main plasma variables. Nozzle/plasma detachment[34–36] in a plasma thruster seems a major theoretical problem, in need of deep revision.[37]

The plasma equations of the quasi-1D model are

$$d(Ag_i)/dz = 0, \quad g_i = n_i u_i, \tag{1}$$

$$d(Am_i u_i g_i)/dz = -en_i A d\phi/dz, \tag{2}$$

$$0 = en_j d\phi/dz - T_j dn_j/dz \quad (j = c,h), \tag{3}$$

$$\epsilon_0 d^2\phi/dz^2 = e(n_c + n_h - n_i), \tag{4}$$

where symbols are conventional. The two electron populations are assumed isothermal (or their temperature varying in a larger scale than the acceleration scale) and ions are considered cold with respect to the temperature T_c of cold electrons.

Carrying out the first-integrals of Eqs. (1)–(3) and using subindex 0 for far-upstream conditions and S for the nozzle throat, one has

$$An_iu_i = \text{const} = G, \quad G = A_S g_S, \tag{5}$$

$$m_i u_i^2/2 + e\phi = 0, \tag{6}$$

$$n_j = n_{j0}\exp(e\phi/T_j) \quad (j = c,h). \tag{7}$$

The small Debye length limit allows us to consider the plasma quasineutral everywhere, with

$$n_i = n_c + n_h \equiv n \tag{8}$$

substituting to Eq. (4), except where a thin non-neutral layer forms; this will be treated as a discontinuity on the quasineutral scale.

The three-species plasma and the solution of the model are characterized by the temperature and upstream-density ratios between the two electron populations,

$$\tau = T_h/T_c, \quad \alpha_0 = n_{h0}/n_0, \tag{9}$$

with $n_0 = n_{c0} + n_{h0}$. Cases with $\alpha_0 = 0$ and 1 (which are equivalent) will be called *simple* plasmas, while cases with $0 < \alpha_0 < 1$ will be called *three-species* plasmas. The practical range of interest is α_0 small, but the whole range of α_0 is considered for the sake of completeness. Parameters n_0 and T_c are used to define dimensionless variables, which, except for the dimensionless electric potential, $\psi = -e\phi/T_c$, are distinguished by an overbar, that is, $\bar{n}_i = n_i/n_0$, $\bar{u}_i = u_i/\sqrt{T_c/m_i}$, etc.

The quasineutral plasma satisfying Eq. (8) may be viewed as a single fluid of velocity, u_i, and pressure and (effective) temperature defined by

$$p = T_h n_h + T_c n_c, \quad T = p/n = (1-\alpha)T_c + \alpha T_h, \tag{10}$$

with

$$\alpha(z) = n_h/(n_c + n_h) \tag{11}$$

the local density fraction of hot electrons. The equation of motion of that fluid is

$$2\frac{d\ln u_i}{dz} = \frac{d\ln(-\phi)}{dz} = \frac{2}{M^2-1}\frac{d\ln A}{dz}, \tag{12}$$

where $M = u_i/c_s$ is the Mach number based on the local sound speed c_s, which is defined by

$$\frac{1}{m_i c_s^2} = \frac{dn}{dp} = \frac{1-\alpha}{T_c} + \frac{\alpha}{T_h}. \tag{13}$$

Notice that in this fluid picture, the electrostatic energy $e\phi$ plays the role of the specific enthalpy in conventional gas dynamics.[10]

Figure 1 shows, for α_0 and τ given, the dependence of plasma magnitudes on the electric potential ψ. The main feature for a three-species plasma is that n_c decreases much faster than n_h with ψ, so that hot-electron properties dominate for ψ large enough; this is illustrated by the change of slope of $n(\psi)$ in Fig. 1(a). As a consequence, the (average) electron temperature T shifts from $\sim T_c$ to $\sim T_h$, Fig. 1(b). It turns out that the local sound speed changes faster with ψ (from $\sim\sqrt{T_c/m_i}$ to $\sim\sqrt{T_h/m_i}$) than the plasma velocity u_i, leading to local extrema of the Mach number observed in Fig. 1(c). The presence of a local minimum of M below 1

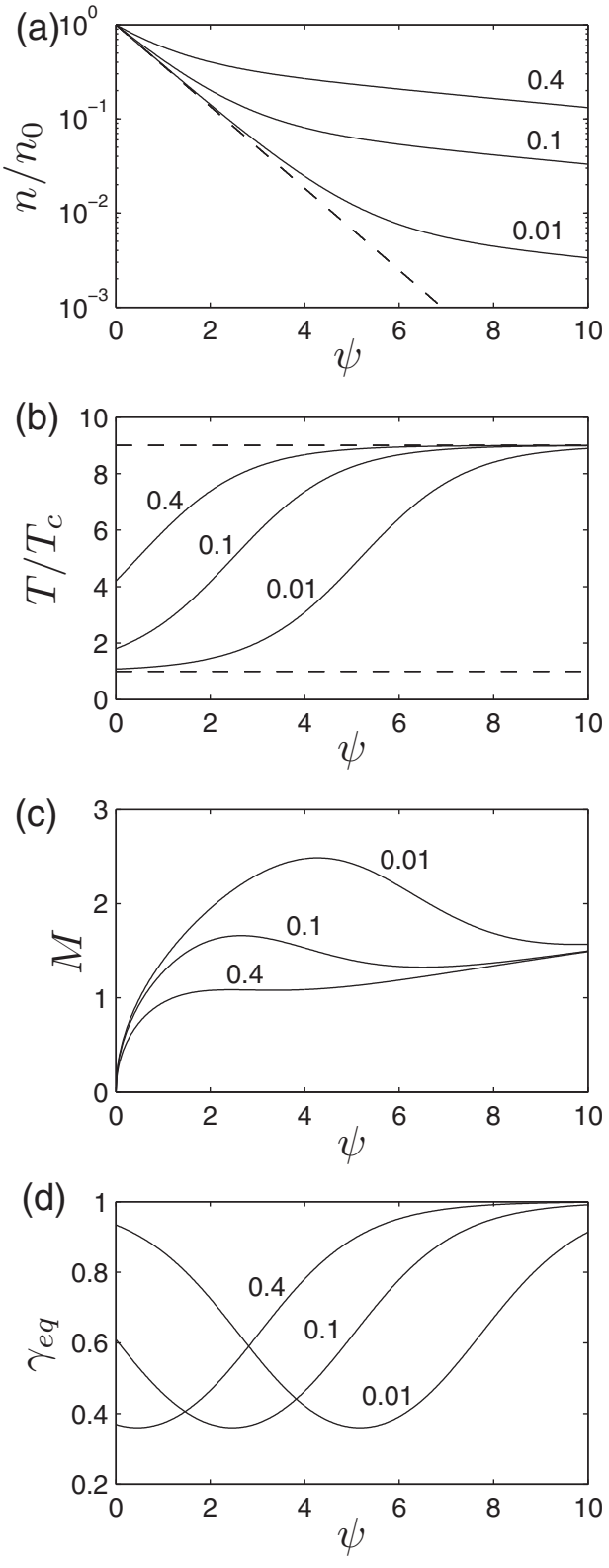

FIG. 1. Thermodynamic properties of a three-species plasma for $\tau = 9$, and $\alpha_0 = 0.01$, 0.1, and 0.4. The dashed line in (a) is for $\alpha_0 = 0$.

and, therefore, of various sonic points will be the cause of the formation of non-neutral layers within the expansion. Another illustration of the *anomalous thermodynamics* of the three-species plasma is the behavior of the 'equivalent specific heat ratio'[10]

$$\gamma_{eq} = d\ln p/d\ln n = m_i c_s^2/T \leq 1. \tag{14}$$

Figure 1(d) shows that $\gamma_{eq}(\psi)$ is close to 1 when one of the two electron species dominate, but presents an intermediate minimum, which tends to zero when $\tau \gg 1$. Since $\gamma_{eq}=1+d\ln T/d\ln n$, to have $\gamma_{eq}<1$ means that the plasma temperature *increases* as its density *decreases*.

Observe that the current-free condition is not a strict assumption in our model. Only the ion current appears explicitly in the equations and is part of the solution. Indeed, the present model is valid for current-carrying plasmas, as long as the driven electron current is much less than the electron thermal current, so that most electrons are effectively confined.

III. PLASMA EXPANSION REGIMES

In dimensionless form, Eqs. (6) and (7) yield

$$\bar{u}_i(\psi) = \sqrt{2\psi}, \quad \bar{n}_c(\psi) = (1-\alpha_0)\mathrm{e}^{-\psi}, \quad \bar{n}_h(\psi) = \alpha_0 \mathrm{e}^{-\psi/\tau}, \tag{15}$$

and the plasma flux for a quasineutral expansion is

$$\bar{g}(\psi) = (\bar{n}_c + \bar{n}_h)\bar{u}_i. \tag{16}$$

The substitution of Eq. (16) into Eq. (5) yields an implicit equation for the potential profile $\psi[A(z)]$, in terms of the area variation,

$$\bar{g}(\psi)/\bar{g}_S = A_S/A(z). \tag{17}$$

The right-hand side of Eq. (17) presents a maximum at the nozzle throat. For the solution to be regular across the throat and assuming that $d\psi/dz|_S \neq 0$, $\bar{g}(\psi)$ must be maximum there. Then, Eq. (12) states that the flow is sonic at the throat, $M_S=1$.

For the plasma expansion to be fully quasineutral, $\bar{g}(\psi)$ must have only a single maximum. The local extrema of $\bar{g}(\psi)$ are the solutions of

$$0 = d\bar{g}/d\psi. \tag{18}$$

There are one or three extrema depending on the values of α_0 and τ.[29] There is a single maximum for any α_0, if τ is below the threshold value $\tau^*=5+\sqrt{24}=9.90$. For $\tau>\tau^*$, there are two maxima (located at $\psi\sim 1/2$ and $\psi\sim\tau/2$) when α_0 is between two limit curves, $\alpha_{0,1}(\tau)$ and $\alpha_{0,2}(\tau)$, that correspond to fulfill

$$d\bar{g}/d\psi = 0, \quad d^2\bar{g}/d\psi^2 = 0, \tag{19}$$

simultaneously, and are plotted in Fig. 2.

In order to separate the spatial gradients caused by the plasma characteristics from those due exclusively to the nozzle shape, $A(z)$, the dimensionless spatial-like variable

$$\zeta = \mathrm{sign}(z)\sqrt{A/A_S - 1} \tag{20}$$

is used. For instance, the local electric field is measured by

$$\frac{d\psi}{dz} = \frac{d\zeta}{dz}\frac{d\psi}{d\zeta}, \tag{21}$$

and the first and second factors on the right-hand side account, respectively, for the contributions of the nozzle shape and the plasma itself. The influence on the electric field of a known nozzle shape is obvious, and certainly an abrupt change of $\zeta(z)$ leads to a QSL (but not to a DL). Our attention here is devoted to profile steepening coming from $d\psi/d\zeta \gg 1$ and caused by a three-species fully-ionized plasma.

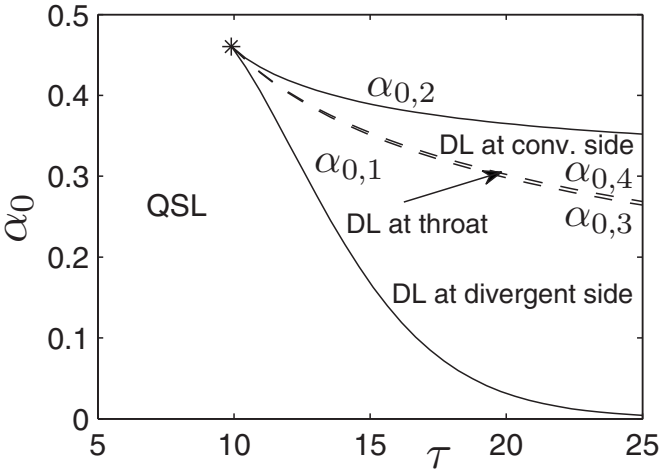

FIG. 2. Parametric regimes in plane (α_0, τ) for the formation of either a QSL or a DL.

In the parametric region where the expansion is fully quasineutral, Eqs. (16) and (18) determine $\psi_S(\tau,\alpha_0)$ and $\bar{g}_S(\tau,\alpha_0)$, thus completing the solution. Figure 3 plots spatial profiles (along ζ) of main plasma magnitudes for different α_0 and $\tau=9$. For the simple plasma with $\alpha_0=0$, one has $\psi_S=1/2$ and $\bar{g}_S=\mathrm{e}^{-1/2}$; for $\alpha_0=1$, it is $\psi_S=\tau/2$ and $\bar{g}_S=(\tau/\mathrm{e})^{1/2}$. As α_0 increases from zero, Figs. 3(a) and 3(b), plotting the electric potential and field, show the formation of a quasineutral steepened layer (QSL) for $\psi(\zeta)$. The profile steepening is observed in all magnitudes that depend on ψ, such as $\bar{n}_c$, $\bar{n}_h$, $\bar{u}_i$, $\bar{T}$, and $\bar{c}_s$. The formation of the QSL takes place mainly at α_0 small (which is the expected practical range) and the maximum steepening is reached around $\alpha_0 \sim 0.3$. For $\alpha_0>0.5$, roughly, the QSL has disappeared and the expansion is almost insensitive to α_0. Notice that small fractions of hot electrons produce large effects: the maximum electric field for $\alpha_0\sim 6\%$ is similar to the one for $\alpha_0>0.5$. As α_0 increases, the location of the QSL moves upstream, but it remains in the divergent side for the main range, $\alpha_0<0.5$. For α_0 small, the QSL is observed only if the nozzle expansion area is large enough.

Figure 3(c) measures the relative density of hot electrons. The QSL acts as an effective barrier for cold electrons; instead, $\bar{n}_h$ remains almost constant upstream of the QSL and dominates the electron population downstream of it. Consistent with the behavior of $\bar{n}_h$, the local sound speed c_s increases across the QSL from $\sim\sqrt{T_c/m_i}$ to $\sim\sqrt{T_h/m_i}$. This abrupt increase explains the minimum of the Mach number M in the QSL region, observed in Fig. 3(d).

The transition from a plasma expansion with an intermediate QSL to an expansion with a non-neutral DL corresponds to the case when the ambipolar electric field in the QSL becomes infinite, $d\psi/d\zeta=+\infty$. This is the condition that leads to Eq. (19) defining the parametric curves $\alpha_{0,1}(\tau)$ and

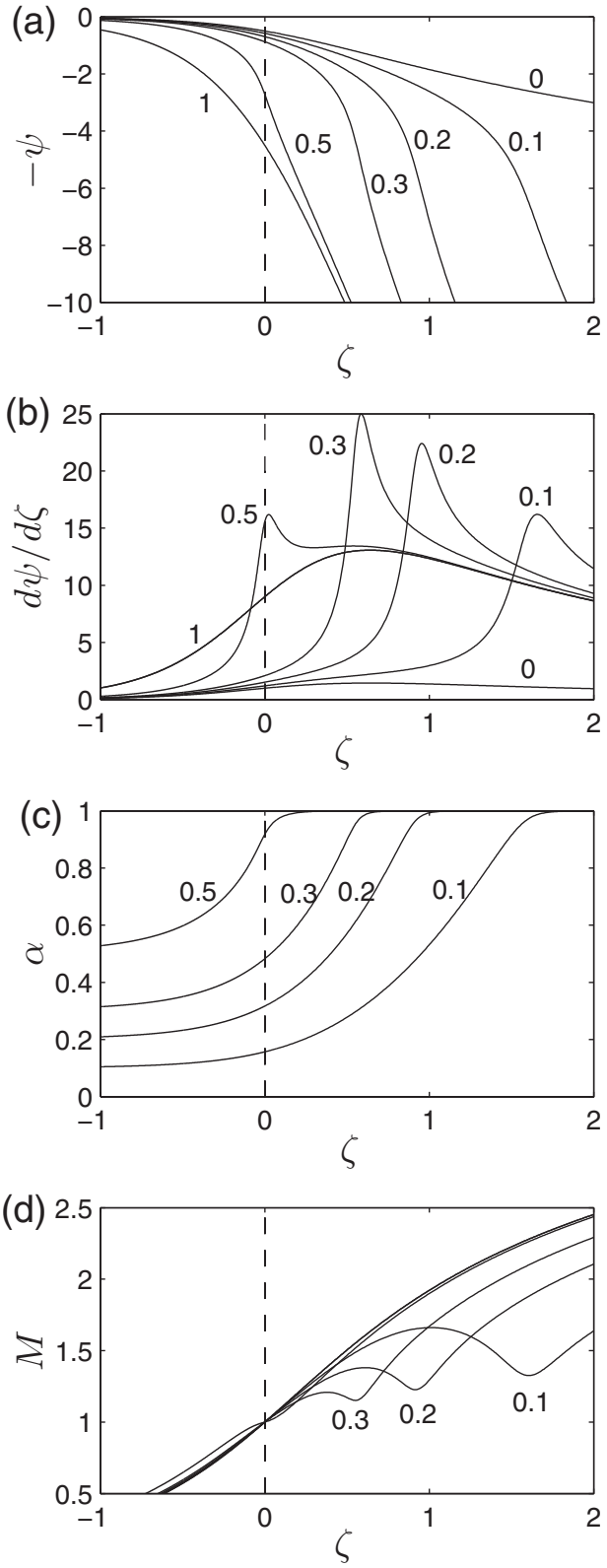

FIG. 3. Spatial variation of (a) plasma potential ($-\psi=e\phi/T_c$), (b) electric field, (c) relative density of hot electrons ($\alpha=n_h/n$), and (d) ion Mach number for $\tau=9$, and $\alpha_0=0$, 0.10, 0.2, 0.3, 0.5, and 1. The spatial-like variable ζ depends on nozzle area expansion. The nozzle throat is at $\zeta=0$.

$\alpha_{0,2}(\tau)$. From Eq. (12), the flow becomes sonic where $d\psi/d\zeta=+\infty$. Therefore, the formation of a DL is linked to the plasma encountering a second sonic point that cannot be crossed in a regular way.

TABLE I. Double layer conditions in the different regimes.

	DL entrance A	DL exit B	DL location
$\alpha_{0,1}<\alpha_0<\alpha_{0,3}$	Supersonic	Supersonic	In divergent side
$\alpha_0=\alpha_{0,3}$	Sonic	Supersonic	A reaches the throat
$\alpha_{0,3}<\alpha_0<\alpha_{0,4}$	Sonic	Supersonic	In nozzle throat
$\alpha_0=\alpha_{0,4}$	Sonic	Sonic	B reaches the throat
$\alpha_{0,4}<\alpha_0<\alpha_{0,2}$	Sonic	Subsonic	In convergent side

An intermediate double layer forms for $\tau>\tau^*$ and $\alpha_{0,1}(\tau)<\alpha_0<\alpha_{0,2}(\tau)$.[29] Indeed, three parametric subregions are distinguished depending on the DL type, the subregions limited by curves $\alpha_{0,3}(\tau)$ and $\alpha_{0,4}(\tau)$ of Fig. 2. Appendix A details the derivation of the solutions for the different double layers. Table I summarizes the DL conditions in the five parametric regions. Points A and B represent the entrance and exit boundaries of the DL.

Figure 4 shows the plasma profiles for $\tau=18$ and different values of α_0, covering cases in all parametric regions. Notice, as α_0 varies, the continuous transition from solutions with a QSL to those with a DL. The continuous transition of the solutions with the temperature ratio τ is illustrated by the comparison of Figs. 3 and 4. The location of the DL moves upstream when either α_0 or τ are increased. Figures 4(c) and 4(d) show the profiles of the Mach number when the DL is located in the divergent and convergent sides, respectively. As in Fig. 3(d), for the DL in the divergent side there is a pronounced minimum of M, reaching values near 1, around the DL; notice that there is no conservation of the Mach number across the DL.

IV. PERFORMANCE AND PROPULSIVE ANALYSIS

A consequence of the isothermal model used for electrons is that for $A\to\infty$, one has $\psi\to\infty$ and $u_i\to\infty$. Of course, there are different phenomena (2D expansion effects, closure of magnetic lines, loss of magnetization, detachment, Coulomb collisions, etc.) that would invalidate the 1D model before $A\to\infty$, but the fact that u_i does not reach a finite limit value downstream constrains our propulsive analysis to *finite nozzles*, i.e., to magnetic nozzles with a finite expansion ratio, $\sigma=A_F/A_S$, with subscript F naming the final section of our nozzle. This limitation should not be very severe for our pursued comparison of plasmas with and without a hot-electron tail. Anyway, the finite nozzle case is the relevant one: for a nozzle that intersects a wall (as in plasma-based material processing[38]); presumably, for a nozzle tested inside a vacuum chamber; or when it covers the region where most of the thrust is imparted.

A. Enhancement of plasma momentum

Figure 5(a) plots, for $\tau=18$, the variation with α_0 of the dimensionless electric potential, $e\phi/T_c$, at the distinguished locations S, A, and B. The broken line S, representing ψ_S, separates the subsonic and supersonic regions of the quasineutral expansion. For τ large but smaller than τ^*, there is a sharp but continuous change of $-\phi_S$ from $\sim T_c/2e$ to

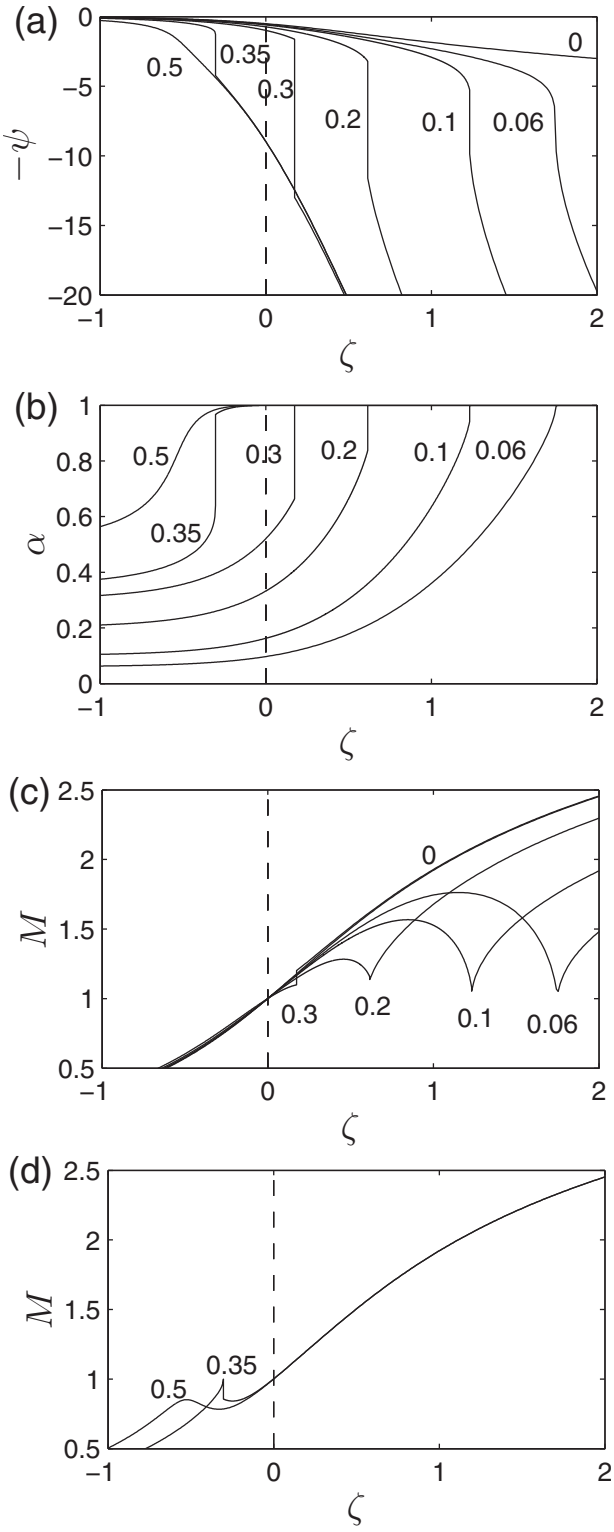

FIG. 4. Spatial variation of (a) plasma potential, (b) relative density of hot electrons, and [(c)–(d)] ion Mach number for $\tau=18$, and $\alpha_0=0$, 0.06, 0.10, 0.20, 0.30, 0.35, and 0.50. A double layer is formed for $\alpha_0=0.10$, 0.20, and 0.30 at the divergent side and for 0.35 at the convergent side.

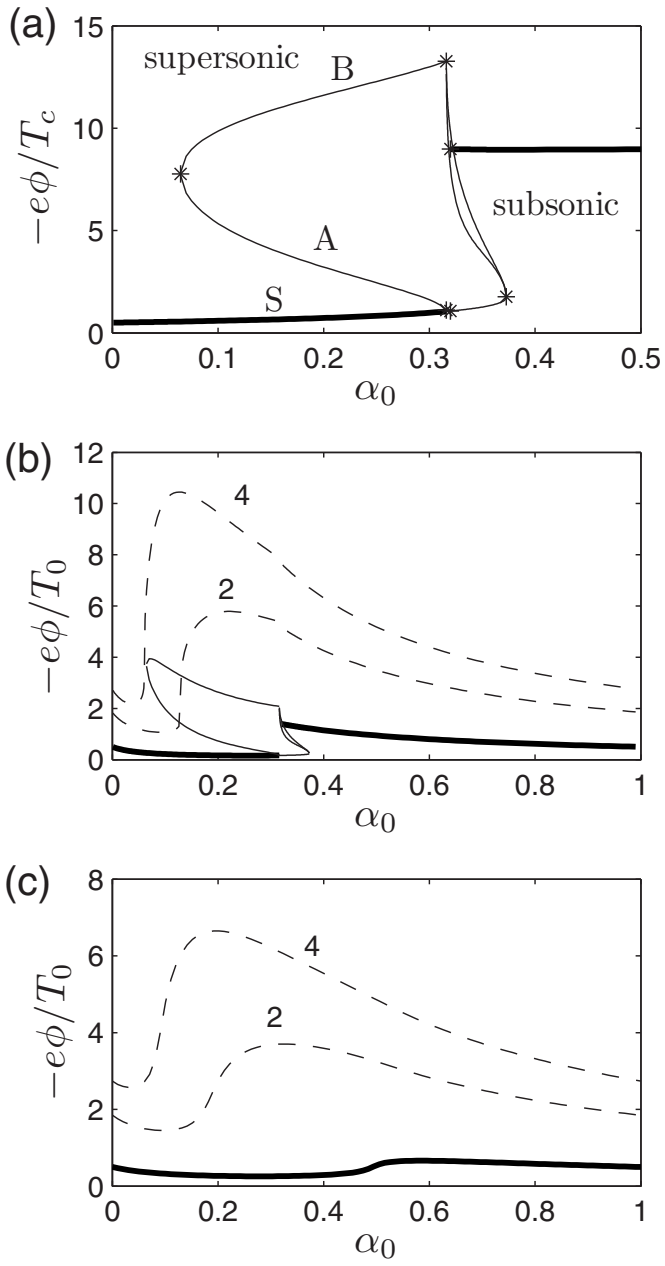

FIG. 5. Plasma potential at distinguished locations for $\tau=18$ in (a) and (b); and $\tau=9$ in (c), normalized with T_c in (a), and with T_0 in (b) and (c). Thick solid lines are for the nozzle throat S, thin solid lines for the DL boundaries A and B, and dashed lines for $A/A_S=2$ and 4. Asterisks in (a) mark the limits of each parametric regime. The horizontal scale of (b) and (c) differs from that of (a).

$\sim T_h/2e$, around $\alpha_0\sim 0.45$. For $\tau>\tau^*$, this change happens in the thin region $\alpha_{0,3}<\alpha_0<\alpha_{0,4}$ when the DL discontinuity is at the throat (although ψ_S is not strictly defined within that region). The potential jump across the double layer is maximum in that region too. In region $\alpha_{0,3}<\alpha_0<\alpha_{0,2}$, we can observe, first, the small rippling of the DL exit values, and second, that point A is a singular sonic point (the regular subsonic/supersonic transition of the plasma being located at the throat S, except for the undefined case of region $\alpha_{0,3}<\alpha_0<\alpha_{0,4}$).

The upstream (average) electron temperature, $T_0=(1-\alpha_0)T_c+\alpha_0 T_h$, is a better normalization parameter than T_c for measuring the relative variation of the electric potential along the nozzle. Figure 5(b) plots, for $\tau=18$, the renormalized potential at points S, A, and B, showing (i) that cases $\alpha_0=0$ and 1 are identical, (ii) the nonmonotonic behavior of $e|\phi_S|/T_0$, and (iii) its abrupt increment when the DL location

crosses the nozzle throat (at $\alpha_0 \simeq \alpha_{0,3}$). Figure 5(c) demonstrates that, for the case of $\tau=9$, with only a QSL, the behavior of $e|\phi_S|/T_0$ is similar to the previous case, with the sharp increment taking place at $\alpha_0 \sim 0.45$, when the QSL crosses the nozzle throat.

Figures 5(b) and 5(c) show how the ion energy per ion, $-e\phi$, increases with the ratio A/A_S in the divergent nozzle (i.e., as the plasma moves downstream). Only a fraction of the ion energy is gained at the steepened layer. For A/A_S given, observe the large increment of $|\phi|$ at a certain α_0. For nozzles with a finite expansion ratio, $\sigma=A_F/A_S$, that potential increment indicates that there is a minimum value of α_0 (i.e., a minimum upstream-density ratio of hot electrons) for the QSL to form within the finite nozzle; that value decreases when σ and τ increase.

The plasma total momentum flux along the nozzle, $F(z)$, sum of the ion and electron contributions, is

$$F(z) = F_i(z) + F_e(z) = m_i n u_i^2 A + pA. \tag{22}$$

In our 1D model, $F(z)$ is identified as the function yielding the increment of thrust along the nozzle. For a finite nozzle, thrust and specific impulse are defined as F_F and $I_{sp}=F_F/\dot{m}$. To compare performances, we consider next plasma beams with the same mass flow $\dot{m}=m_i A_S g_S$ and upstream (average) temperature T_0. Then, reference values for plasma momentum and density, based on $\dot{m}$ and T_0 (instead of n_0 and T_c), are

$$F_* = \dot{m} c_0, \quad n_* = \dot{m}/(A_S m_i c_0), \tag{23}$$

with $c_0=\sqrt{T_0/m_i}$ [not to be mistaken with the local sound speed c_{s0}, Eq. (13)]. By fixing $\dot{m}$: first, we cancel the obvious effect of the beam size, so that thrust and specific impulse behave in the same way; and second, the upstream plasma density n_0 becomes an output parameter, controlled by the choking of the plasma flow at the throat.

Figures 6(a)–6(c) show parameters characterizing the plasma expansion in the convergent nozzle as a function of α_0 for two values of τ. Figure 6(a) plots the ratio n_0/n_*: it is equal to $e^{1/2}$ for a simple plasma, but it can be considerably larger for a three-species plasma, which means a higher choking for the same $\dot{m}$. For $\tau > \tau^*$, the maximum value of n_0/n_* takes place when the DL reaches the throat from the divergent side. Figure 6(b) plots the normalized plasma momentum flux at the nozzle throat, F_S/F_*, which behaves similar to n_0/n_*. Finally, Fig. 6(c) depicts the relative contribution of ion momentum to F_S. As expected, it is $F_{iS}=F_{eS}=F_S/2$ for a simple plasma. The same result is found for a three-species plasma when the DL is in the convergent side, implying that at the throat the plasma is already a 2-species one. On the contrary, F_{iS}/F_S can be considerably smaller than 1/2 when the DL or QSL are located in the divergent nozzle (i.e., for small values of α_0). Observe that: the behavior of F_{iS}/F_S follows that of n_*/n_0; and $F_{iS}/F_{eS}=m_i c_{sS}^2/T_S$ so that $F_{iS}/F_{eS}<1$ reflects the fact that the 'equivalent specific heat ratio', Eq. (14), is smaller than 1.

Figures 7(a) and 7(b) plot the spatial variation of the plasma momentum flux in the divergent nozzle, illustrating the two main actions of that nozzle region: (a) the conversion of electron momentum into ion momentum and (b) the increase of plasma momentum. The most relevant features are, first, the abrupt increase of ion momentum across a QSL or a DL, and, second, the *zero change* of plasma momentum across a DL. This last property, well-known in double layer theory,[25–28] is immediate from the plasma momentum equation

$$\frac{dF}{dz} = \frac{\epsilon_0}{2}\frac{d}{dz}\left(\frac{d\phi}{dz}\right)^2 + p\frac{dA}{dz}, \tag{24}$$

which is obtained from Eqs. (2)–(4). The first term in the right-hand side yields the variation of F within the double layer, which *cancels out* at the two DL sides, i.e., $F_A=F_B$.

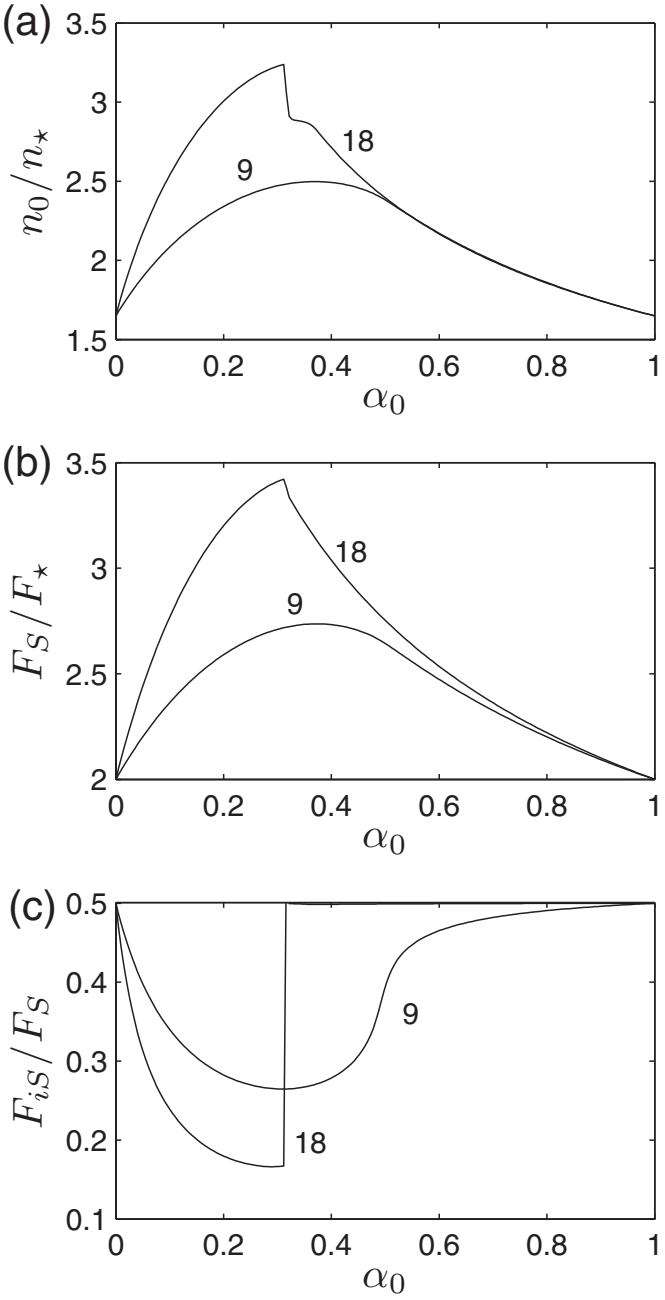

FIG. 6. Plasma response in the convergent side of the nozzle vs α_0, for $\tau=9$ and 18. (a) Upstream plasma density (for a given mass flow), (b) plasma momentum flux at the throat, and (c) relative contribution of ions to the plasma momentum flux at the throat.

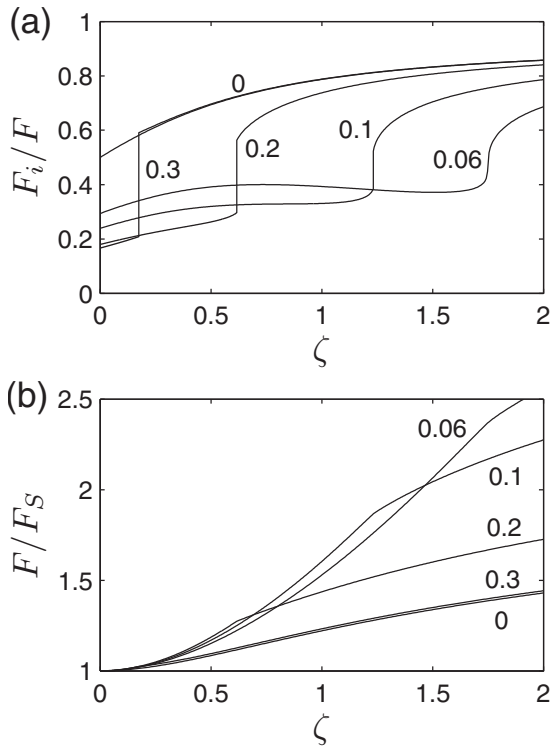

FIG. 7. Variation of plasma momentum flux in the divergent nozzle for $\tau=18$ and $\alpha_0=0$, 0.06, 0.1, 0.2, and 0.3: (a) relative contribution of ion momentum flux; (b) increase of plasma momentum flux relative to the value at the throat.

Therefore, a DL just converts electron momentum into ion momentum and does not constitute by itself a mechanism for imparting thrust. On the contrary, the supersonic plasma expansion in the divergent nozzle *does* increment the thrust, as Fig. 7(b) illustrates. Nonetheless, the physical thrust mechanisms are different in solid and magnetic nozzles. In classical gas dynamics flowing inside solid nozzles, the thrust comes from the pressure on the diverging walls. In a magnetic nozzle the pressure gradient at the plasma/vacuum edge generates a diamagnetic azimuthal current, and the Lorentz force associated to that current on the nozzle magnetic circuit produces the thrust.[7]

Once the DL has been disregarded as a thrust mechanism, the point that remains to be discussed is whether a three-species plasma still presents any propulsive gain over a simple plasma. Figure 8(a) plots the specific impulse relative to the upstream sound velocity for different three-species plasmas and two finite nozzles. Notice that I_{sp}/c_0 is equivalent to F_F/F_* and is sometimes called the thrust coefficient.[39] The increase of the thrust coefficient that corresponds to the divergent side of the nozzle, i.e., F_F/F_S, can be inferred from Figs. 8(a) and 6(b). The thrust coefficient I_{sp}/c_0 increases with the expansion ratio, as expected. More interestingly, (i) it reaches a marked maximum with α_0 corresponding always to the steepened layer located in the divergent nozzle, and (ii) it does not increase with τ when the steepened layer is on the convergent nozzle.

In order to compare three-species plasmas with simple plasmas, Fig. 8(b) plots the ratio of I_{sp} versus $I_{sp,0}$, the specific impulse of the simple plasma *with the same* T_0. The ratio $I_{sp}/I_{sp,0}$ is closely related to $(e|\phi_F|/T_0)^{1/2}$, plotted in Figs. 5(b) and 5(c). Figure 8(b) emphasizes the fact that the performances of a three-species plasma differ from those of a simple plasma only when the steepened layer is on the divergent nozzle. Since the equivalent specific ratio γ_{eq} is a function of α_0 [Fig. 1(d)], the dependence of I_{sp} on α_0 of Fig. 8(b) bears a resemblance to the dependence of the specific impulse I_{sp} on the specific heat ratio, γ, in isentropic gas dynamics,[39] where $\partial I_{sp}/\partial\gamma<0$, although the effect of γ_{eq} is stronger here.

B. Thrust efficiency

Figure 8(b) seems to suggest that three-species plasmas present a large gain in specific impulse (up to a factor of ~2 in the figure) with respect to simple plasmas. However, a comparison based on the same T_0 is not valid to assess the propulsive quality of different collisionless plasmas, since they can require very different power deposition, P_d, to reach the same T_0. Here lies an important difference between chemical and electric thrusters. In a chemical thruster, the specific power, $P_d/\dot{m}$, is an intrinsic property of the propellant, the upstream temperature is set locally and satisfies $T_0 \propto P_d/\dot{m}$; thus, comparisons based on the same $P_d/\dot{m}$ or the same T_0 are similar. In electric thrusters, the available power P_d comes from an external source (through electrodes or antennas) and, more importantly, for near-collisionless plasmas, the temperature of the *confined* electrons is not determined locally but comes out from an energy balance (at kinetic level) on the whole expansion region;[33] this relates in a very different way T_0 to $P_d/\dot{m}$.

Therefore, a correct assessment of the propulsive quality of a plasma/thruster system must consider plasmas with the same $\dot{m}$, same P_d, and same nozzle. Then, the appropriate propulsive parameter is the thrust efficiency,

$$\eta = F_F^2/2\dot{m}P_d = I_{sp}^2\dot{m}/2P_d. \tag{25}$$

The power deposited in the plasma can be split into useful power, P_{use}, and power losses. In our limited 1D model for a finite nozzle and a current-free plasma, the useful power is the downstream plasma (ion plus electron) power,

$$P_{use} = \left(\frac{u_{iF}^2}{2} + 2a\frac{T_F}{m_i}\right)\dot{m},$$
$$a = \frac{1+(\tau^{3/2}-1)\alpha}{[1+(\tau-1)\alpha][1+(\tau^{1/2}-1)\alpha]}. \tag{26}$$

Here, the expression of parameter a must be seen as a simple estimate only; it is based on the assumption of a similar behavior of the high-energy tails of cold and hot electrons in a three-species plasma, and it is $a=1$ for a simple plasma. For a nozzle with a large expansion ratio, the electron contribution to P_{use} is small and the uncertainties on the expression of a should not matter much.

The contributions to power losses are ionization and radiation, wall deposition, plume divergence, and detachment. Their analysis is outside of the possibilities of our model so that the comparison here must be limited to plasmas with the

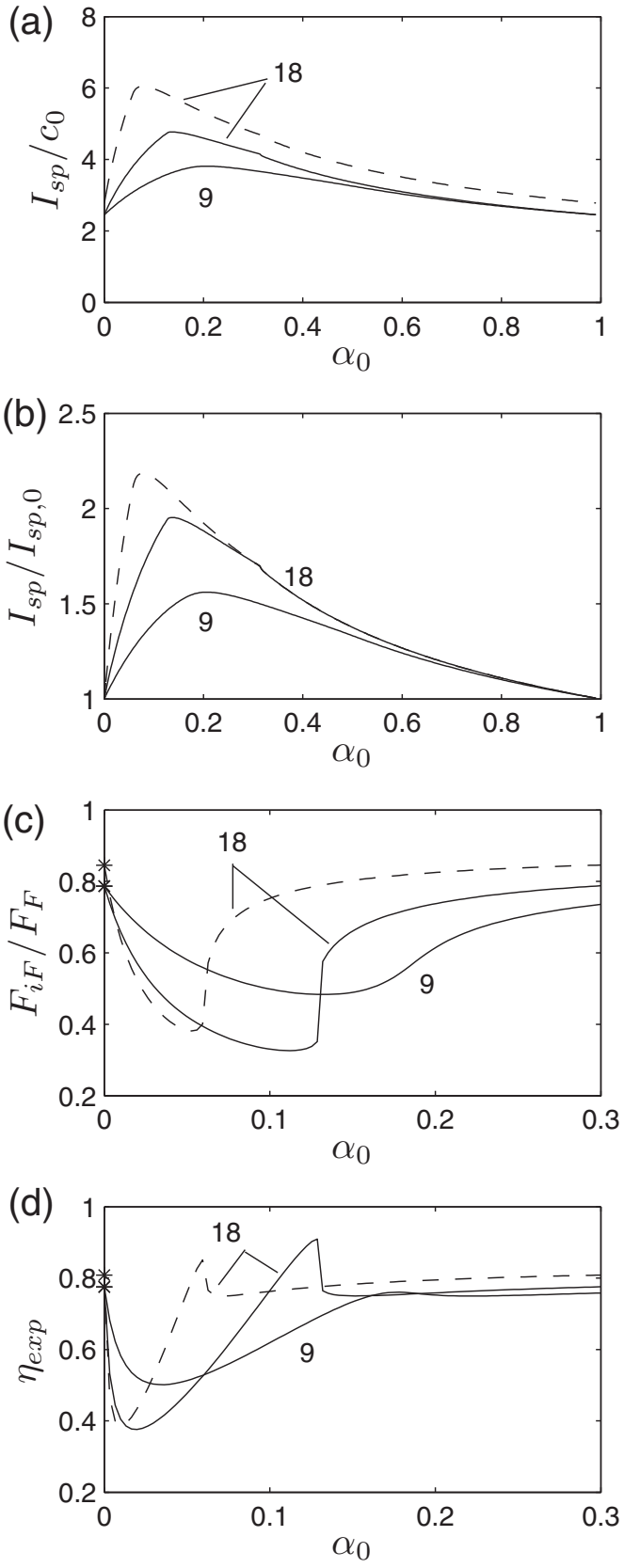

FIG. 8. Propulsive figures vs α_0, for $\tau=9$ and 18, and $\sigma=2$ (solid lines) and 4 (dashed lines). (a) Specific impulse coefficient, (b) specific impulse of a three-species plasma referenced to that of a simple plasma with the same T_0, (c) ion momentum contribution to the thrust, and (d) expansion efficiency. Asterisks in (d) represent values for a simple plasma. Notice that the horizontal scale in (c) and (d) differs from that of (a) and (b).

same useful power. For this class of plasmas, the thrust efficiency is factorized as

$$\eta = \eta_{loss}\eta_{exp}, \quad \eta_{loss} = P_{use}/P_d, \quad \eta_{exp} = I_{sp}^2/I_{sp,m}^2, \tag{27}$$

where $I_{sp,m}=(2P_{use}/\dot{m})^{1/2}$, and the expansion efficiency η_{exp} is the only factor that can be analyzed here. We find

$$1-\eta_{exp} = \frac{2\mu-1}{\mu(\mu+4a)} = \frac{2}{\mu} + O\left(\frac{1}{\mu^2}\right), \tag{28}$$

with $\mu=F_{iF}/F_{eF}$. If M_F is the Mach number at the end of the nozzle, one has $\mu<M_F^2$ for a three-species plasma and $\mu \simeq M_F^2$ when the hot population dominates downstream. Figure 8(c) plots the ion contribution to thrust, $F_{iF}/F_F=\mu(1+\mu)^{-1}$ and Fig. 8(d) plots η_{exp}. From these figures we conclude that, in general, a three-species plasma presents a lower expansion efficiency than a simple plasma, the deficit being maximum in the case of higher interest, when the steepened layer is in the divergent nozzle.

Apart from the efficiency of the 1D expansion, the thrust efficiency of plasmas with and without hot electrons can still differ because of power losses, due to either processes inside the source (ionization and wall heating) or 2D effects in the downstream part of the nozzle (radial energy and detachment). At present, all these processes are very poorly known for a three-species plasma.

The fact that $\eta_{exp}<1$ is due to the incomplete expansion of the plasma in the finite nozzle. Indeed, the isothermal assumption makes η_{exp} increase very slowly with σ. Adiabatic cooling of electrons[33] is likely to make $\eta_{exp}(\sigma)$ approach one much quicker, so that $I_{sp}\simeq I_{sp,m}$ independently of the plasma parameters, α_0 and τ. Then, the difference in thrust efficiency between plasmas with and without hot electrons would lie exclusively on aspects outside the scope of the present model.

The isothermal assumption also implies that, for $\sigma\to\infty$, $M_F(\sigma)\to\infty$. For plasmas with $\dot{m}$ and $P_{use}=\eta_{loss}P_d$ given, the plasma velocity tends to $I_{sp,m}$, and therefore, the upstream temperature satisfies $T_0(\sigma)\to 0$. This is consistent with the global energy balance that determines T_0 in a collisionless plasma (of course, the 1D model is not expected to apply for $\sigma\to\infty$). Then, for $\dot{m}$ and P_{use} given, the curves of Fig. 8(a) are not informing us on the variation of I_{sp} but of $T_0\eta_{exp}^{1/2} \approx T_0$, and the curves of Fig. 8(b) are depicting (approximately) the ratio $\sqrt{T_0/T_{0,0}}$, with $T_{0,0}$ the upstream temperature of the simple plasmas with the same P_{use}.

V. CONCLUSIONS

The presence of two electron populations in a fully-ionized collisionless plasma leads to an anomalous thermodynamic behavior, illustrated by an equivalent specific ratio lower than one (implying temperature increasing when density decreasing) and a nonmonotonic behavior of the Mach number. A steepened layer is formed around a local minimum of the Mach number and, for α_0 small, marks the transition from a region dominated by cold electrons to a region governed by hot electrons. A two-scale asymptotic analysis is able to distinguish between a quasineutral steepened layer

and a non-neutral double layer. This last one forms when the quasineutral solution presents several sonic points, and a regular crossing of all of them is impossible.

The three-species plasma has been assumed to expand in a convergent-divergent nozzle. For α_0 small, the steepened layer forms in the divergent nozzle, provided that the nozzle expansion ratio is high enough. As α_0 increases, the steepened layer moves toward the throat and the convergent nozzle. In this last case, all three-species effects are confined upstream of the nozzle throat and the downstream plasma is basically a simple one. The formation of the steepened layer in the downstream region of the nozzle leads to a large increment of the total potential fall, from $O(T_c/e)$ to $O(T_h/e)$, and therefore of the energy of ions.

The propulsive properties of the plasma/nozzle system, that is, thrust and specific impulse, are determined by the downstream plasma momentum flux and velocity. It is confirmed that there is no gain in plasma momentum across the DL, just conversion of electron momentum into ion momentum, so that the DL does not constitute a thrust mechanism, as claimed in the HDLT concept. The thrust mechanism in a helicon thruster is the axial Lorentz force between the plasma and the magnetic circuit, independently of whether the ion acceleration takes place in a very thin DL or gradually along the divergent nozzle.

A comparative propulsive analysis for simple and three-species plasmas has been carried out under the constraints of same useful power, mass flow, and finite magnetic nozzle. Although the study of the power losses related to plasma processes inside the source and in the 2D detachment region remains to be done, we have found no indication that the presence of a hot-electron tail makes the plasma more favorable for propulsion. Indeed, we find that, for any finite nozzle, the expansion efficiency is, in general, slightly lower for a three-species plasma than for a simple plasma.

The formation of a QSL in a three-species plasma has been confirmed by a 2D model of a magnetic nozzle.[40] There, the QSL is observed as a curved front with a pronounced peak of the ambipolar electric field and the parametric dependence of the QSL location and potential agrees with present results. The 2D model is purely quasineutral and could not be run within the CFDL parametric region. With respect to propulsive efficiency, the 2D model concludes that the plume efficiency, defined as the ratio of axial-to-total ion power, is slightly lower for a three-species plasma.

We acknowledge that the simple Boltzmann relation used for cold and hot electrons is the most delicate aspect of our model. First, the cold electron population is likely to be Maxwellian upstream of the nozzle throat but magnetic moment effects modify that character on the divergent nozzle.[33] Second and more relevant for the study here, there is no reliable knowledge of the upstream distribution function of hot electrons. Solutions with a CFDL have been found using monoenergetic populations of hot electrons[13,16] and polytropic laws for the two electron populations.[10] This would mean that the DL, being a local structure, is not much dependent on the details of the upstream distribution functions (as long as cold and hot electron energies are disparate). On the contrary, the downstream properties of the (collisionless) plasma, such as the final plasma velocity and the density profile, are certainly influenced by the hot-electron distribution function and the presence of intermediate energy barriers (related to either the DL, magnetic moments, or a moving plasma boundary[33]).

Finally, the present model can be easily extended to include the ionization and heating processes in the upstream side of the nozzle. Then, several conservation laws that are analytical in the present model would remain differential equations to be integrated numerically. However, as long as ionization and plasma heating are efficient (which is essential for a competitive thruster device), the plasma response in the divergent nozzle, which is the important region in our study, is not modified.

ACKNOWLEDGMENTS

This work was initiated under project 'Helicon Plasma Hydrazine Combined Micro', financed by the European Community (Seventh Framework Programme, Grant No. 218862), and could be finished thanks to the Air Force Office of Scientific Research, Air Force Material Command, USAF, under Grant No. FA8655-10-1-3085. Marginal funding came from the Gobierno de España (Plan Nacional de I+D, Project No. ESP2007-62694). The author thanks Professor Martínez-Sánchez for very fruitful discussions and Dr. Birkan for his support.

APPENDIX A: EXPANSION WITH AN INTERMEDIATE DOUBLE LAYER

The derivation here is extracted from Ref. 29, adding some explanatory details. The internal structure of the DL requires us to solve the Poisson Eq. (4) in the inner variable $\xi=(x-x_{DL})/\lambda_D$, with x_{DL} an inner point of the DL and $\lambda_D=\sqrt{\epsilon_0 T_c/e^2 n_0}$. Equation (4) yields the first integral

$$\frac{1}{2}\left(\frac{d\psi}{d\xi}\right)^2=\int_{\psi_A}^{\psi}(\bar{n}_i-\bar{n}_c-\bar{n}_h)(\psi)d\psi\equiv U(\psi)-U(\psi_A) \tag{A1}$$

with

$$U(\psi,\bar{g}_A;\alpha_0,\tau)=\sqrt{2\psi}\bar{g}_A+\bar{n}_c(\psi)+\tau\bar{n}_h(\psi), \tag{A2}$$

the (dimensionless) Sagdeev's potential. Since a non-neutral DL connects two quasineutral regions of the plasma, a steady DL inside any plasma must satisfy the following three pairs of conditions at its upstream and downstream boundaries (points A and B, respectively):[26,25] (a) plasma quasineutrality, $U'=0$; (b) asymptotically zero space-charge field, $U_B=U_A$ [in order to cancel the total DL charge and match with the much weaker ambipolar field of the quasineutral regions]; and (c) the sonic/supersonic Bohm condition, $U''\geq 0$, which assures the development of a nonoscillatory layer profile. In terms of the function $\bar{g}$, these *necessary* conditions imply that $\bar{g}_A=\bar{g}_B$, and $\bar{g}'_A,\bar{g}'_B\leq 0$. Physically, the last conditions imply that the ion flow cannot be subsonic at the entrance and exit of a *standard* DL.

A standard DL forms for $\alpha_{0,1}(\tau)<\alpha_0<\alpha_{0,3}(\tau)$ on the divergent nozzle. The ion flow is supersonic at both the DL

entrance and exit. For (τ, α_0) given, the DL is defined by three parameters: the ion flux $\bar{g}_A$ across it and the entrance and exit potentials ψ_A and ψ_B. These are obtained from the set of algebraic equations

$$\bar{g}_A = \bar{g}(\psi_A) = \bar{g}(\psi_B), \quad U_B(\psi_B, \bar{g}_A) = U_A(\psi_A, \bar{g}_A), \tag{A3}$$

and Eq. (17) yields the location of the DL. Figures 3(a)–3(b) of Ref. 29 plot the inner profiles of such DL. As α_0 is increased, the DL location moves upstream. The limit curve $\alpha_0 = \alpha_{0,3}(\tau)$ is determined from the additional condition $d\bar{g}/d\psi|_A = 0$ and corresponds to the case when the DL entrance reaches the throat and the ion flux at the DL entrance is sonic.

Reference 29 discusses that the fulfillment of all conditions for a standard DL is impossible in the parametric region $\alpha_{0,3}(\tau) < \alpha_0 < \alpha_{0,2}(\tau)$. Instead, an 'ill-ended' DL is formed, which is constituted by the usual monotonic region, from entrance A to an intermediate point C where ϕ is minimum and the ion flux is subsonic, followed by a (space-charged) rippled tail. This type of DL is illustrated in Figs. 3(c)–3(d) of Ref. 29 and has been reported also in the wall-collection models of Refs. 13, 15, and 16. Parameters $\bar{g}_A$, ψ_A, and ψ_C determining the monotonic part of the DL are obtained from

$$\bar{g}_A = \bar{g}(\psi_A), \quad \bar{g}'(\psi_A) = 0, \quad U_B(\psi_C, \bar{g}_A) = U_A(\psi_A, \bar{g}_A). \tag{A4}$$

Then, the electron density at point C is

$$\bar{n}_{eC} = (1 - \alpha_0)e^{-\psi_C} + \alpha_0 e^{-\psi_C/\tau} \tag{A5}$$

and, because of the potential barrier created around the minimum potential ψ_C, the electron density is constant in the rippled tail. This modifies the Sagdeev's potential there, that becomes $U = \sqrt{2\psi\bar{g}_A} - \psi\bar{n}_{eC}$.

Since the space-charge rippling is small and averages to zero in distances Δz, such that $\lambda_d \ll \Delta z \ll L$, it makes sense to consider the averaged plasma profiles downstream of the monotonic part of the DL. This requires us to define the 'exit' of the DL as a point B with averaged values in the rippled tail. It turns out that the potential ψ_B defining point B is

$$\psi_B = \bar{u}_{iB}^2/2 \equiv (\bar{g}_A/\bar{n}_{eC})^2/2. \tag{A6}$$

In the quasineutral region downstream of the DL, the electron densities of Eq. (15) are modified into

$$\bar{n}_c = (1 - \alpha_0)e^{\psi_{CB} - \psi}, \quad \bar{n}_h = \alpha_0 e^{(\psi_{CB} - \psi)/\tau}, \tag{A7}$$

with $\psi_{CB} = \psi_B - \psi_C$. Physically, these modifications are the consequence of the potential barrier for electrons at the rippled tail.

The DL with a rippled tail covers the whole parametric region $\alpha_{0,3} < \alpha_0 < \alpha_{0,2}$, but two subregions are distinguishable in terms of the location of the double layer: they are separated by the curve $\alpha_0 = \alpha_{0,4}(\tau)$ of Fig. 2. For $\alpha_{0,4} < \alpha_0 < \alpha_{0,2}$, the double layer is located in the convergent side of the nozzle, whereas for $\alpha_{0,3} < \alpha_0 < \alpha_{0,4}$, the whole DL is at the nozzle throat. The curve $\alpha_0 = \alpha_{0,4}(\tau)$ is obtained imposing that the exit of a DL reaches the throat from the convergent side, which means to impose the extra condition $\bar{g}'(\psi_B) = 0$, with the electron densities satisfying Eq. (A7).

[1] C. Charles and R. Boswell, Appl. Phys. Lett. **82**, 1356 (2003).
[2] T. Ziemba, J. Carscadden, J. Slough, J. Prager, and R. Winglee, *41st Joint Propulsion Conference*, Tucson, AR (American Institute of Aeronautics and Astronautics, Washington, D.C., 2005), p. 4119.
[3] O. Batishchev, IEEE Trans. Plasma Sci. **37**, 1563 (2009).
[4] D. Pavarin, F. Ferri, M. Manente, D. Curreli, Y. Guclu, D. Melazzi, D. Rondini, S. Suman, J. Carlsson, C. Bramanti, E. Ahedo, V. Lancellotti, K. Katsonis, and G. Markelov, *31st International Electric Propulsion Conference*, Ann Arbor, MI (Electric Rocket Propulsion Society, Fairview Park, OH, 2009), p. 205.
[5] A. Gurevich, L. Pariiskaya, and L. Pitaevskii, Sov. Phys. JETP **22**, 449 (1966).
[6] S. A. Andersen, V. O. Jensen, P. Nielsen, and N. D'Angelo, Phys. Fluids **12**, 557 (1969).
[7] E. Ahedo and M. Merino, Phys. Plasmas **17**, 073501 (2010).
[8] C. Charles and R. Boswell, Phys. Plasmas **11**, 1706 (2004).
[9] C. Charles, R. Boswell, and M. Lieberman, Appl. Phys. Lett. **89**, 261503 (2006).
[10] B. Bezzerides, D. W. Forslund, and E. L. Lindman, Phys. Fluids **21**, 2179 (1978).
[11] L. M. Wickens, J. E. Allen, and P. T. Rumsby, Phys. Rev. Lett. **41**, 243 (1978).
[12] A. Gurevich, D. Anderson, and H. Wilhelmsson, Phys. Rev. Lett. **42**, 769 (1979).
[13] L. Schott, Phys. Fluids **30**, 1795 (1987).
[14] K. Sato and F. Miyawaki, Phys. Fluids B **4**, 1247 (1992).
[15] A. Kono, J. Phys. D **32**, 1357 (1999).
[16] T. E. Sheridan, P. Chabert, and R. W. Boswell, Plasma Sources Sci. Technol. **8**, 457 (1999).
[17] G. Hairapetian and R. L. Stenzel, Phys. Fluids B **3**, 899 (1991).
[18] X. Sun, A. Keesee, C. Biloiu, E. Scime, A. Meige, C. Charles, and R. Boswell, Phys. Rev. Lett. **95**, 025004 (2005).
[19] S. A. Cohen, X. Sun, N. Ferraro, E. E. Scime, M. Miah, S. Stange, N. Siefert, and R. Boivin, IEEE Trans. Plasma Sci. **34**, 792 (2006).
[20] N. Plihon, P. Chabert, and C. S. Corr, Phys. Plasmas **14**, 013506 (2007).
[21] P. Zhu and R. W. Boswell, Phys. Fluids B **3**, 869 (1991).
[22] R. T. S. Chen and N. Hershkowitz, Phys. Rev. Lett. **80**, 4677 (1998).
[23] A. W. Degeling, T. E. Sheridan, and R. W. Boswell, Phys. Plasmas **6**, 1641 (1999).
[24] S. Tysk, C. Denning, J. Scharer, and K. Akhtar, Phys. Plasmas **11**, 878 (2004).
[25] L. Block, Astrophys. Space Sci. **55**, 59 (1978).
[26] M. A. Raadu, Phys. Rep. **178**, 25 (1989).
[27] V. Lapuerta and E. Ahedo, Phys. Plasmas **7**, 2693 (2000).
[28] A. Fruchtman, Phys. Rev. Lett. **96**, 065002 (2006).
[29] E. Ahedo and M. Martínez-Sánchez, Phys. Rev. Lett. **103**, 135002 (2009).
[30] F. F. Chen, Phys. Plasmas **13**, 034502 (2006).
[31] A. Fruchtman, G. Makrinich, and J. Ashkenazy, Plasma Sources Sci. Technol. **14**, 152 (2005).
[32] E. Ahedo, *31st International Electric Propulsion Conference*, Ann Arbor, MI (Electric Rocket Propulsion Society, Fairview Park, OH, 2009), p. 193.
[33] A. Arefiev and B. Breizman, Phys. Plasmas **15**, 042109 (2008); **16**, 055707 (2009).
[34] R. W. Moses, R. Gerwin, and K. Schoenberg, *Proceedings Ninth Symposium on Space Nuclear Power Systems*, Albuquerque, NM, 1992, AIP Conf. Proc. No. 246 (American Institute of Physics, Woodbury, NY, 1992), pp. 1293–1303.
[35] E. B. Hooper, J. Propul. Power **9**, 757 (1993).
[36] A. Arefiev and B. Breizman, Phys. Plasmas **12**, 043504 (2005).
[37] E. Ahedo and M. Merino, *46th Joint Propulsion Conference*, Nashville, TN (American Institute of Aeronautics and Astronautics, Washington, D.C., 2010), p. 6613.
[38] K. Schoenberg, R. Gerwin, R. Moses, J. Scheuer, and H. Wagner, Phys. Plasmas **5**, 2090 (1998).
[39] G. Sutton and O. Biblarz, *Rocket Propulsion Elements*, 7th ed. (Wiley, New York, 2001).
[40] M. Merino and E. Ahedo, *Proceedings of Space Propulsion 2010*, San Sebastián, Spain, 3–6 May 2010 (European Space Agency, Noordwijk, The Netherlands, 2010), p. 1841391; "Simulation of plasma flows in divergent magnetic nozzles," IEEE Trans. Plasma Sci. (submitted).